

Interphase Engineering Enhanced Electro-chemical Stability of Prelithiated Anode

Shiwei Xu, Qiu Fang, Jipeng Wu, Suting Weng, Xiaoyun Li, Qiuyan Liu, Qiyu Wang, Xiqian Yu, Liqun Chen, Yejing Li, Zhaoxiang Wang,* and Xuefeng Wang*

Prelithiation is an essential technology to compensate for the initial lithium loss of lithium-ion batteries due to the formation of solid electrolyte interphase (SEI) and irreversible structure change. However, the prelithiated materials/electrodes become more reactive with air and electrolyte resulting in unwanted side reactions and contaminations, which makes it difficult for the practical application of prelithiation technology. To address this problem, herein, interphase engineering through a simple solution treatment after chemical prelithiation is proposed to protect the prelithiated electrode. The used solutions are carefully selected, and the composition and nanostructure of the as-formed artificial SEIs are revealed by cryogenic electron microscopy and X-ray photoelectron spectroscopy. The electrochemical evaluation demonstrates the unique merits of this artificial SEI, especially for the fluorinated interphase, which not only enhances the interfacial ion transport but also increases the tolerance of the prelithiated electrode to the air. The treated graphite electrode shows an initial Coulombic efficiency of 129.4%, a high capacity of 170 mAh g⁻¹ at 3 C, and negligible capacity decay after 200 cycles at 1 C. These findings not only provide a facile, universal, and controllable method to construct an artificial SEI but also enlighten the upgrade of battery fabrication and the alternative use of advanced electrolytes.

1. Introduction

Lithium-ion batteries (LIBs) are dominantly used in electric vehicles, portable devices, electric grids, etc., and the demand for LIBs with a higher energy density and longer cycling life is increasing.^[1] To increase the energy density, on one hand, researchers are dedicated to pushing the capacity limit of both cathode and anode materials by rising the upper charge voltage while minimizing the loss of active Li inventory.^[2] On the other hand, electrode materials with higher energy density such as silicon (Si)-based anodes and Li metal are going to use but will suffer from severe side reactions and capacity loss due to their increased reactivity with the electrolyte and large volume changes.^[3] For example, the irreversible Li loss of graphite (Gr) anode is at a range of 5–20% (corresponding to an initial Coulombic efficiency (ICE) of 95–80%) while that of Si-based anodes is enlarged to be 30–50%.^[3b,4] Consequently, extra Li supply enabled by prelithiation technology becomes necessary to compensate for such

irreversible Li loss and thus to increase the energy density and cycle life of LIBs.^[5]

Based on the type of Li resources and reaction mechanisms, additional Li can be prestored in the materials/electrodes through either additive, electrochemical, chemical, or physical contact methods.^[6] With the increased Li concentration inside, the prelithiated materials/electrodes become more reactive and readily react with air and electrolyte, resulting in unwanted side reactions and contaminations.^[7] This will not only deteriorate the electrochemical performance of the electrodes but also demand additional setups and cost to safely handle and transfer these reactive prelithiated materials/electrodes, which increases the difficulty for the practical application of prelithiation technology.^[8] To solve this problem, protecting the highly reactive materials/electrodes with a passivation layer is essential, such as Li₂O/Li₂CO₃ coating on the Li_xSi particles.^[6e,9] However, the electro-chemo-mechanical property of the protective layers and their synthesis methods should be finely tuned to have the following merits: 1) chemically and electrochemically stable, 2) dense to protect from air contamination, 3) ionically conductive, and 4) easy fabrication.^[10]

S. Xu, Q. Fang, J. Wu, S. Weng, X. Li, Q. Liu, Q. Wang, X. Yu, L. Chen, Y. Li, Z. Wang, X. Wang
Beijing National Laboratory for Condensed Matter Physics
Institute of Physics
Chinese Academy of Sciences
Beijing 100049, China
E-mail: zwxwang@iphy.ac.cn; wxf@iphy.ac.cn

S. Xu, S. Weng, Z. Wang, X. Wang
School of Physical Sciences
University of Chinese Academy of Sciences
Beijing 100190, China

Q. Fang, J. Wu, X. Li, Q. Liu, Z. Wang, X. Wang
College of Materials Science and Opto-Electronic Technology
University of Chinese Academy of Sciences
Beijing 100190, China

X. Wang
Tianmu Lake Institute of Advanced Energy Storage Technologies Co.
Ltd
Liyang, Jiangsu 213300, China

 The ORCID identification number(s) for the author(s) of this article can be found under <https://doi.org/10.1002/smll.202305639>

DOI: 10.1002/smll.202305639

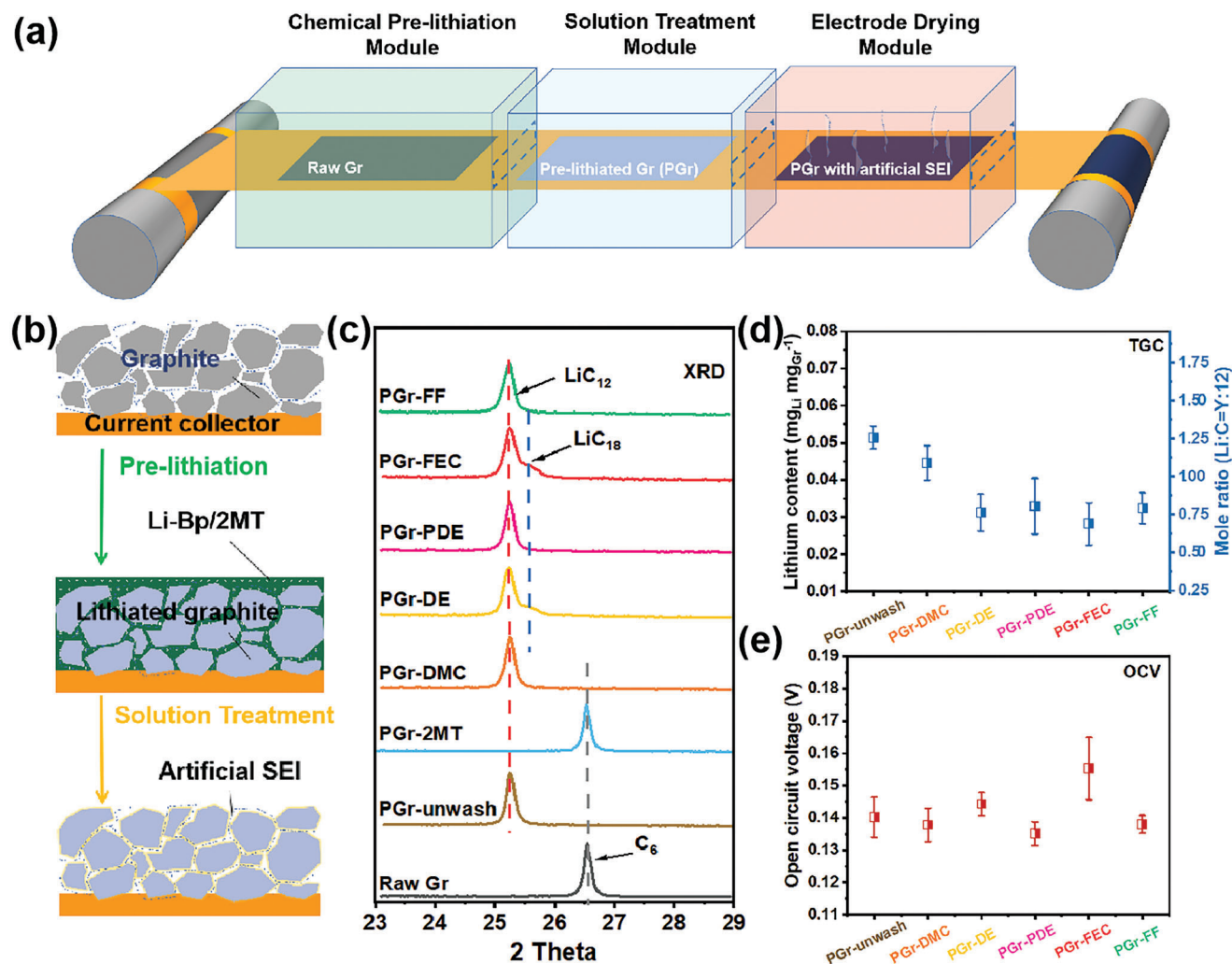


Figure 1. a) Schematic diagram for process line of chemical prelithiation and artificial SEI construction. b) Schematic diagram for electrode changes during above processes. c) XRD patterns of graphite electrodes after different treatments. d) TGC-measured Li^+ content in the graphite electrodes after different treatments. e) OCV variations of coin cells assembled with different graphite electrodes.

With these regards, herein, we are aiming to construct an artificial solid electrolyte interphase (SEI) on the prelithiated electrode, which not only meets the above requirements but also approaches an ideal SEI thus improving ICE, cycling performance, and rate performance of battery concurrently. It was simply prepared by the reaction between a functional solution and the prelithiated electrodes or/and trace residual organolithium used for chemical prelithiation. The composition and nanostructure of the as-formed artificial SEI can be adjusted by using various solutions and revealed by cryogenic electron microscopy (cryo-EM), electron energy loss spectroscopy (EELS), and X-ray photoelectron spectroscopy (XPS). Especially, the prelithiated graphite electrode with artificial LiF-rich interphase shows an ICE of 129.4%, a high capacity of 170 mAh g^{-1} at 3 C, and negligible capacity decay after 200 cycles at 1 C, much better than the untreated one. These findings not only provide a facile, universal, and controllable method to construct an artificial SEI but also enlighten current prelithiation technology upgrades to integrate into practical battery fabrication.

2. Results and Discussions

2.1. Process Line for Chemical Prelithiation and Artificial SEI Construction

Considering the potential compatibility with the current battery fabrication line, chemical prelithiation is preferred followed by a solution treatment to construct an artificial SEI while removing the residual organolithium reagents. **Figure 1a** shows the corresponding process line consisting of three modules where the raw electrode is first prelithiated in the “chemical prelithiation module,” then transferred to the “solution treatment module” to form artificial SEI, and finally dried in the “electrode drying module.” Graphite electrode was used as a model anode since it is still dominantly used in the commercial LIBs, and Li dissolving in biphenyl-2-methyl tetrahydrofuran (Li-Bp/2MT) solution was used for chemical prelithiation reagents (1 mol L^{-1}). Given the high reactivity of both organolithium reagent and prelithiated graphite,^[11] spontaneous chemical reactions take place

when they are in contact with some conventional organic solvents and electrolytes, thus forming artificial SEI on the surface of graphite particles (Figure 1b). This solution-based treatment is facile, controllable, and prone to forming a homogeneous coating layer, while the physical and chemical properties of artificial SEI can be finely tuned by altering the solution compositions and reaction pathways.

As shown in Figure 1c, chemical prelithiation of the graphite electrode in Li-Bp/2MT for 10 min results in the formation of the LiC₁₂ phase^[12] as evidenced by X-ray diffraction (XRD) patterns. However, using 2MT to wash the prelithiated graphite electrode can erase the prestored Li⁺ probably due to the weak chemical bonding between intercalated Li⁺ and graphene layers (Figure S1, Supporting Information), indicating that 2MT is not a suitable solvent to rinse the prelithiated graphite electrode. In contrast, using some regular organic solvents and electrolytes can well maintain the prestored Li⁺ in the graphite structure. Meanwhile, they are expected to form an artificial SEI on the graphite surface, including dimethyl carbonate (DMC), a mixture of DMC and ethylene carbonate (EC) (DE, DMC:EC = 1:1 vol%), 1 mol L⁻¹ lithium hexafluorophosphate (LiPF₆) in DE solution (PDE), fluoroethylene carbonate (FEC), and 1 mol L⁻¹ lithium bis(fluorosulfonyl)imide LiFSI in FEC (FF). The resultant graphite electrodes are denoted as PGr-solvent/electrolyte, such as PGr-FF. The content of prestored Li⁺ in the graphite structure is an important factor for prelithiation technology and was quantified by titrated gas chromatography (TGC) measurements^[13] (Figure 1d), which are 0.05, 0.045, 0.03, 0.035, 0.028, and 0.03 mg_{Li} mg_{Gr}⁻¹ for PGr-unwash, PGr-DMC, PGr-DE, PGr-PDE, PGr-FEC, and PGr-FF, respectively. This order is inversely consistent with the sequence of the open-circuit voltage (OCV, Figure 1e) when these treated graphite electrodes were assembled in the coin cells as a higher Li⁺ concentration leads to a lower OCV. Compared with the unwashed one, the lower Li⁺ content in the PGr-solvents/electrolytes implies that some active Li participated and consumed in the reactions forming artificial SEI or be cleared away with residual organolithium reagents.

2.2. Prelithiation and Artificial SEI-Enhanced Electrochemical Performance

The electrochemical performance of the graphite electrodes after prelithiation and solution treatment was evaluated in half cells and shown in Figure 2 and Figure S2 (Supporting Information). The original graphite electrode exhibits an initial discharge-specific capacity (IDSC) of 446 mAh g⁻¹ and an initial charge-specific capacity (ICSC) of 382 mAh g⁻¹ (Figure 2a,b), corresponding to a capacity loss of 65 mAh g⁻¹ and an ICE of 86% (Figure 2c) due to the SEI formation. Chemical prelithiation can compensate for such capacity loss (Figure 2b) and increase the ICE by over 100% (Figure 2c). Nevertheless, improper washing using 2MT could not only disable the prelithiation but also have a negative effect on the electrochemical performance of graphite electrode, leading to higher polarization (Figure 2a), lower reversible capacity, and ICE (Figure 2a,d). The prestored Li ions are well preserved in the graphitic structure after special solution treatments and can be electrochemically extracted during charging, yielding extra charge capacity named compensated lithium

capacity (CLC) and ICEs of more than 110% (Figure 2c). Although DMC and DE treating prelithiated graphite electrodes exhibit extremely high ICE over 150%, lower reversible capacity (<301 mAh g⁻¹) and higher polarization are obtained (Figure 2a), which indicates that the formed artificial SEIs have low ionic conductivity and thus increase the cell resistance (Figure 2g). In contrast, the prelithiated graphite electrodes treated with FEC, PDE, and FF display high reversible capacity and low polarization comparable to the raw one.

The long-term effect of different solution treatments was evaluated by the cycling performance (Figure 2d,h; Figure S2a,b, Supporting Information) and rate performance (Figure 2e,f). Without any treatment, the raw graphite electrode displays a capacity gradually decreased to 350 mAh g⁻¹ after 50 cycles (Figure 2d). Although slowly increased during the first 20 cycles due to the interphase reconstruction (referred to as detachment/dissolution/oxidation and reformation; Figure S2c–f, Supporting Information), the reversible capacity of PGr-DMC and PGr-DE is still lower than 350 mAh g⁻¹. In contrast, PGr-PDE, PGr-FEC, and PGr-FF exhibit stable cycling performance with a high reversible capacity of ≈365 mAh g⁻¹. When the current is varied from 0.2 to 3 C (1 C = 372 mA g⁻¹), PGr-FF displays the highest capacity retention (Figure 2e) and CE (Figure 2f), demonstrating its faster ion transportation enabled by the specially designed artificial SEI. At 3 C, the reversible capacity of these graphite electrodes is in the order of PGr-FF > PGr-FEC > PGr-PDE > PGr-DE > Raw > PGr-2MT > PGr-DMC > PGr-unwash (Figure 2e), suggestive of the essential role of artificial SEI in regulating the reaction kinetic of graphite electrode, especially at the high rates. Based on the electrochemical impedance spectra (EIS) (Figure 2g) and their fitting results (Table S1, Supporting Information), lower interfacial resistance is achieved with FF and PDE treatment when compared with those treated with DMC, DE, and without any treatment (Raw Gr). After 200 cycles at 1 C, PGr-FF and PGr-FEC exhibit the capacity retention of 108.1% and 109.6%, respectively, while it is only 76.1% for the raw one (Figure 2h).

2.3. Nature of the Artificial SEI

Although prelithiation improves the ICE of graphite electrodes, the largely enhanced cycling and rate performance are owing to the presence of specially designed artificial SEI (Figure 3a), which facilitates interfacial Li⁺ transport and charge transfer. To reveal the nature of these artificial SEIs, X-ray photoelectron spectroscopy (XPS), cryo-transmission electron microscopy (cryo-TEM), and electron energy loss spectroscopy (EELS) were applied to probe the chemical components and microstructure of the artificial SEIs on the prelithiated graphite electrodes.

Compared with the almost clean surface of the raw graphite (Figure S3, Supporting Information), solution treatments form artificial SEIs consisting of organic and inorganic species (Figure 3; Figure S4, Supporting Information). Organic-rich interphase is found on the PGr-DE as its XPS signal from organic carbon ROCO₂Li (286.8, 288.6, and 289.8 eV) and ROLi (286.8 eV) is strong (Figure 3b). Besides organic species, LiF is present on the surface of PGr-FEC (Figure 3c). With lithium salts, e.g., LiPF₆ or LiFSI in the solution, they are participated in the

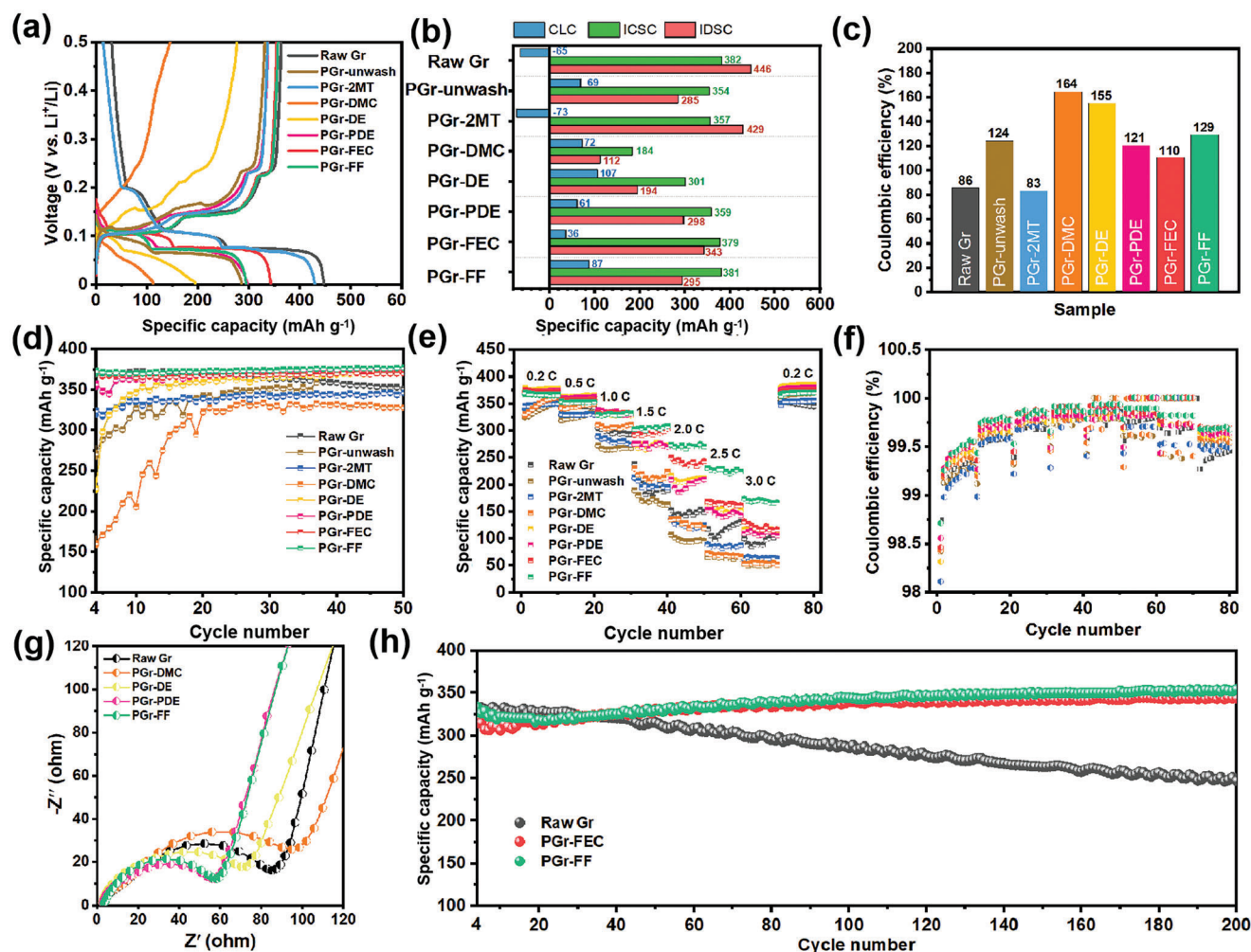


Figure 2. Electrochemical performance of the graphite electrode after different treatments. a) Capacity–voltage curves at the first cycle. b) Initial discharge-specific capacity (IDSC), initial charge-specific capacity (ICSC), and their reduction named compensated lithium capacity (CLC) of graphite electrode at the first cycle. c) Initial Coulombic efficiency (ICE). d) Cycling performance at 0.2 C. e) Rate performance. f) The corresponding CEs at various current rates ranging from 0.2 to 3 C. g) EIS spectra of Raw Gr, PGr-DMC, PGr-DE, PGr-PDE, and PGr-FF after one cycle. h) Long cycling performance at 1 C of Raw Gr, PGr-FEC, and PGr-FF. All the cells for cycling performance and rate performance tests were precycled at 0.05 C (1 C = 372 mA g⁻¹) for three cycles.

reactions and contribute to forming more inorganics in the artificial SEIs, such as LiF (Figure 3b), Li_xPO_yF_z (Figure 3b,f), and other P (Figure 3f), N (Figure 3e), and S (Figure 3d)-containing species. The presence of these components was further confirmed by the attenuated total reflectance-Fourier transform infrared (ATR-FTIR) spectroscopy (Figure S5, Supporting Information), and the potentially involved reaction processes between Li-Bp/2MT and solvents/salts are displayed in Figure S6 (Supporting Information). Consequently, elemental Li and F are dominant on the surfaces of PGr-PDE and PGr-FF and their artificial SEIs are rich in LiF (Figure 3g; Figure S7, Supporting Information). Such inorganic-rich artificial SEI is believed beneficial for fast Li⁺ transport.^[14]

In particular, the nanostructure of the artificial SEI on PGr-FF was revealed by cryo-TEM and EELS (Figure 4; Figure S9, Supporting Information). Based on the characteristic lattice spacings, crystalline LiF and Li₂CO₃ nanograins were identified in the

high-resolution TEM (HRTEM) image (Figure 4a) and its corresponding fast Fourier Transform (FFT) pattern (Figure 4a, inset). They are in irregular shapes, and their particle size is in a range of 5–20 nm. These inorganic particles are distributed closely on the amorphous organic substrates exhibiting a mosaic structure rich in grain boundaries, which could facilitate the Li⁺ transport across the interface and lead to fast reaction kinetics.^[15] EELS spectra of Li (Figure 4b), C (Figure 4c), and F *K*-edge (Figure 4d) confirm the composite nature of this artificial SEI layer consisting of LiF, Li₂CO₃, and organic species like ROLi and ROCO₂Li. The thickness of the artificial SEI layer is estimated to be ≈20 nm by elemental distribution based on their EELS signals (Figure 4e–i) that F (Figure 4h) and O (Figure 4g) are dominant in the artificial SEI layer on the surface (Figure 4i) while Li (Figure 4f) is present in the graphite bulk and surface. The dense coverage of the artificial SEI layer (Figure S9, Supporting Information) can act as a passivation layer protecting the reactive

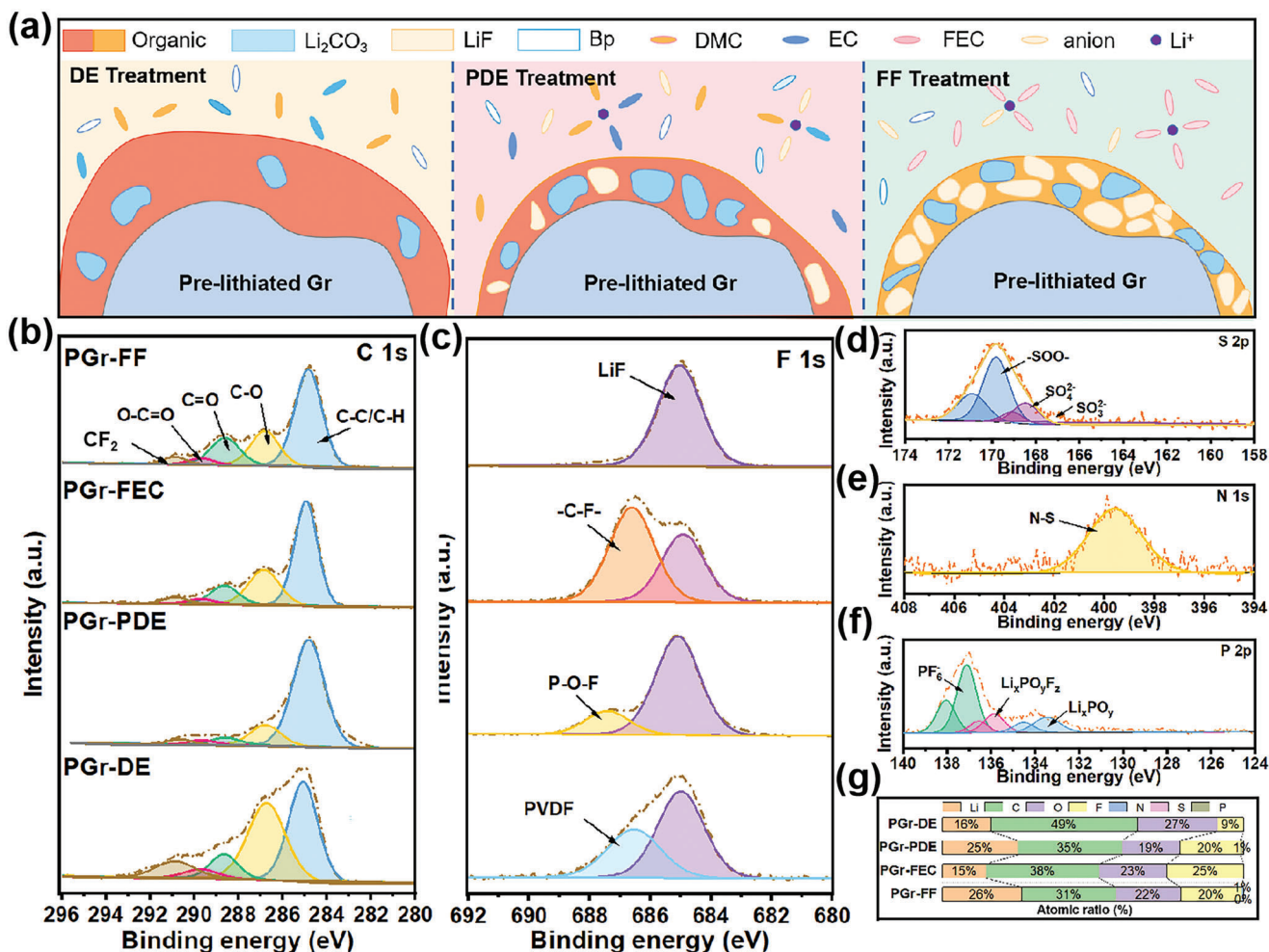


Figure 3. a) Schematic diagram of artificial SEIs on the solution-treated prelithiated graphite electrodes. XPS spectra of b) C 1s and c) F 1s from PGr-DE, PGr-PDE, PGr-FEC, and PGr-FF. XPS spectra of d) S 2p and e) N 1s from PGr-FF. XPS spectrum of f) P 2p from PGr-PDE. g) Relative atomic elemental content of Li, C, O, and F from PGr-DE, PGr-PDE, PGr-FEC, and PGr-FF based on survey spectra (Figure S4, Supporting Information). The LiF in the PGr-DE is from the decomposition products of polyvinylidene difluoride (PVDF) after prelithiation (Figure S8, Supporting Information).

prelithiated graphite particles from external attacks from air and electrolytes during storage and operation.

2.4. Practical Applications

With these artificial SEIs, the storage stability of the prelithiated graphite electrode in the dry room is much enhanced (Figure 5a), which is crucial for practical fabrication and application.^[16] Electrochemically lithiated graphite (discharged to 0.14 V, EGr-0.14 V) with a conventional SEI layer on the surface is unstable when exposed to the ambient air conditions (moisture < 3%) for 10 min, and its phase is converted from LiC₁₂ to graphite as evidenced by the XRD spectra (Figure 5a). This irreversible structural degradation can be largely inhibited by the presence of artificial SEIs, which are stable in dry air (Figure S10, Supporting Information) and can preserve the prestored Li⁺ in the graphitic structure (Figure 5a). When these electrodes were

assembled into coin cells, they exhibit comparable electrochemical performance (Figure 5b,c) to those without air exposure, indicating the negligible influence of air exposure enabled by the specially designed artificial SEI layers on the prelithiated graphite. In contrast, a capacity delay occurs within 40 cycles for the air-exposed electrochemically lithiated graphite (Figure 5c), demonstrating outstanding merits of these artificial SEIs when compared with the traditional electrochemically formed SEI.

The benefit of prelithiation with artificial SEI can be found in the practical full cells demonstrated with LiFePO₄ (LFP) as the cathode and PGr-FF as the anode. Compared to the LFP||Raw Gr, LFP||PGr-FF displays higher ICE (94.9% vs 82.2%) and dramatically improved cycling stability (capacity retention after 200 cycles: 77% vs 36%, Figure 5d). After 200 cycles, a reversible capacity of 107.2 mAh g⁻¹ is achieved for LFP||PGr-FF, almost triple that for LFP||Raw Gr (42.2 mAh g⁻¹). This strategy also works for other anode materials, such as nano-Si, which exhibits enhanced cycling performance than the raw one (Figure 5e).

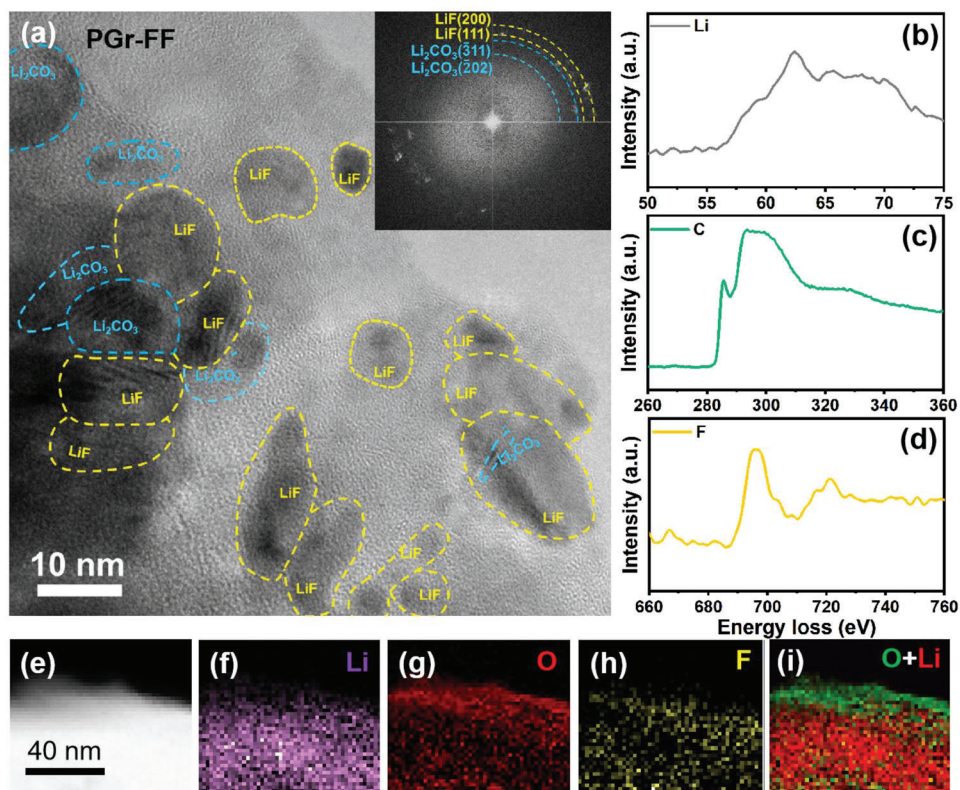


Figure 4. Nanostructure of the artificial SEI layer on the PGr-FF visualized by cryo-TEM. a) HRTEM image, EELS spectra of b) Li K-edge, c) C K-edge, and d) F K-edge, e) STEM image, and elemental distribution of f) Li, g) O, h) F, and i) their overlapped image.

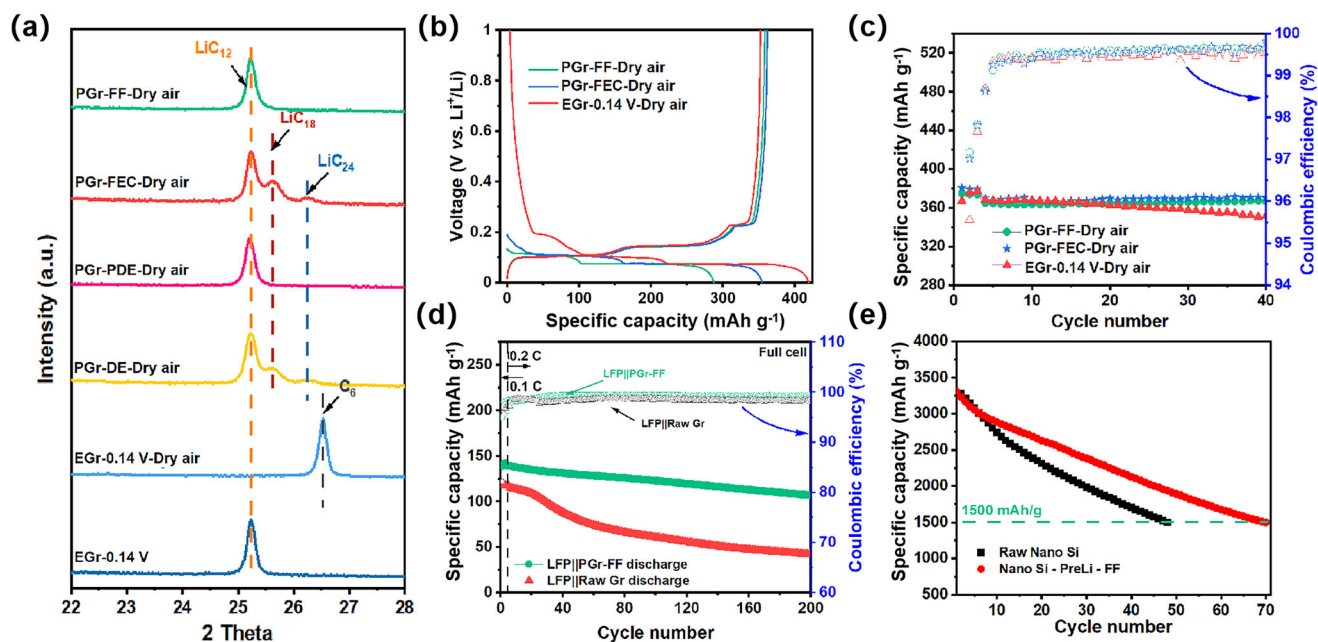


Figure 5. a) XRD patterns of PGr-FEC, PGr-FF, and EGr-0.14 V before and after air exposure for 10 min. b) Capacity–voltage curves and c) cycling performance of the half cells at 0.2 C with PGr-FEC, PGr-FF, and EGr-0.14 V after air exposure. d) Cycling performance of the full cells with LFP as the cathode. e) Cycling performance of nano-Si anode with/without prelithiation and artificial SEI constructed in FF solution at 100 mA g⁻¹.

3. Conclusion

A sequential two-step solution treatment was proposed for chemical prelithiation and artificial SEI construction on anode electrodes for LIBs. Artificial SEI is formed by the reaction between a special solution and residual organolithium/prelithiated electrode and its component and structure of artificial SEI can be adjusted by using different solutions, in which adding lithium salts increases the content of inorganics in the artificial SEI. Such treatment can well maintain the prestored Li^+ in the structure and enhance the tolerance of the prelithiated electrode to the air. Furthermore, the resultant inorganics-rich artificial SEI facilitates interfacial ion transport and contributes to the improved cycling and rate performance of graphite anode. In particular, the prelithiated graphite electrodes with a LiF-rich artificial SEI display an ICE of 129.4%, a high capacity of 170 mAh g^{-1} at 3 C, and negligible capacity decay after 200 cycles at 1 C, much better than the untreated one. This strategy is proved feasible for other anode materials, such as nano-Si. These findings not only provide a facile, universal, and controllable method to construct an artificial SEI but also enlighten the upgrade of battery fabrication and the alternative use of advanced electrolytes.

4. Experimental Section

Materials Availability: Graphite (99.9%, Aladdin), lithium foil (99.9%, GanfengLithium), biphenyl (99%, Alfa), 2-methyl tetrahydrofuran (99%, Innochem), dimethyl carbonate (99%, Aladdin), ethylene carbonate (99%, Aladdin), fluoroethylene carbonate (99%, Aladdin), lithium hexafluorophosphate (99.9%, DoDoChem), lithium bis(fluorosulfonyl)imide (99.9%, DoDoChem).

Materials' Preparation: For chemical prelithiation of graphite electrode, these electrodes were prepared by evenly coating the slurry (90 wt% graphite and 10 wt% polyvinylidene fluoride) on a thin copper foil, followed by drying in air at 60 °C for 6 h then drying in the vacuum at 120 °C for overnight. The as-prepared graphite electrodes were prelithiated by immersing them into 1 mol L^{-1} lithium-biphenyl in the 2-methyl tetrahydrofuran (mole ratio of Li:biphenyl was 1:1) for 10 min and taken out for further solution treatment.

For artificial SEI construction, the prelithiated electrodes were directly immersed in the functional solutions for 10 min and then rinsed with 2-methyl tetrahydrofuran twice. Finally, the electrodes were dried in the vacuum at 60 °C for 2 h. All procedures including chemical prelithiation and solution treatment were carried out in an argon-filled glove box.

Materials' Characterizations: The crystal structure of the samples was determined by XRD (Bruker D8 Advance Diffractometer) with Cu-K α radiation ($\lambda = 1.541 \text{ \AA}$) and 2θ range of 10°–50°. The lithium content in the electrode was measured by TGC measurements with the Nexis GC-2030 GC system equipped with a barrier ionization discharge (BID) detector. First, the prelithiated electrodes were sealed in bottles with rubber cushions through which deionized water (DIW) was injected and reacted with the prelithiated graphite for 30 min to ensure that the reaction was completed. The sampling gas was harvested and measured by GC. The mass of active lithium was estimated based on the content of H_2 . The XPS characterization was implemented on a ThermoFisher ESCALAB 250 Xi with monochromatic 150 W Al K α radiation. All the samples were transferred from the glove box to the XPS chamber using a sealed vessel to avoid exposure to air. The morphologies of the samples were characterized by scanning electron microscope (SEM) (HITACHI S-4800). Cryo-TEM characterizations were carried out using a JEOL JEM-F200 microscope under cryogenic temperatures (–180 °C) at 200 kV. Different prelithiated graphite samples were scraped from the electrodes, rinsed by 2MT, and then loaded

on the TEM grids. A cryo-transfer holder (Fischione 2550) was employed which enabled to safe transfer of the samples from the glove box into the TEM without any air exposure. The structure of graphite and other species was analyzed using Digital Micrograph (DM, Gatan) software.

Electrochemical Measurements: The active material loading of the graphite electrode was $\approx 2.5 \text{ mg cm}^{-2}$. The R2032 coin cells were assembled with an electrolyte of 1 mol L^{-1} LiPF_6 in a mixture of DMC and EC (1:1, vol%) in an argon-filled glove box. The full cells were assembled using commercialized LiFePO_4 as the cathode (80 wt% LFP, Likai, Taiwan, 10 wt% carbon black, and 10 wt% polyvinylidene fluoride), Raw Gr and PGr-FF as the anode, and 1 mol L^{-1} LiPF_6 in EC and DMC (1:1, vol%) as the electrolyte. The capacity ratio of anode to cathode (N/P) was about 1.1:1. Galvanostatic charge and discharge tests were carried out on the NEWARE Battery Testing System. EIS tests were carried out on the Biologic SAS SP-200 electrochemical workstations.

Supporting Information

Supporting Information is available from the Wiley Online Library or from the author.

Acknowledgements

This work was supported by the Natural Science Foundation of Beijing (Grant No. Z200013), the National Natural Science Foundation of China (NSFC No. 52172257), and the National Key Research and Development Program of China (Grant No. 2022YFB2502200).

Conflict of Interest

The authors declare no conflict of interest.

Data Availability Statement

The data that support the findings of this study are available from the corresponding author upon reasonable request.

Keywords

artificial solid electrolyte interphase (SEI), graphite anodes, lithium-ion batteries, prelithiation

Received: July 5, 2023

Revised: August 8, 2023

Published online:

- [1] a) X. Meng, X. Q. Yang, X. Sun, *Adv. Mater.* **2012**, *24*, 3589. b) A. Cresce, K. Xu, *Carbon Energy* **2021**, *3*, 721.
- [2] J. W. Choi, D. Aurbach, *Nat. Rev. Mater.* **2016**, *1*, 16013.
- [3] a) D. Lin, Y. Liu, Y. Cui, *Nat. Nanotechnol.* **2017**, *12*, 194. b) G. Zhu, D. Chao, W. Xu, M. Wu, H. Zhang, *ACS Nano* **2021**, *15*, 15567. c) X. Yi, Y. Feng, A. M. Rao, J. Zhou, C. Wang, B. Lu, *Adv. Mater.* **2023**, *35*, 2302280.
- [4] a) Y. X. Yao, C. Yan, Q. Zhang, *Chem. Commun.* **2020**, *56*, 14570. b) L. Zhao, B. Ding, X. Y. Qin, Z. Wang, W. Lv, Y. B. He, Q. H. Yang, F. Kang, *Adv. Mater.* **2022**, *34*, 2106704.
- [5] a) F. Wang, B. Wang, J. Li, B. Wang, Y. Zhou, D. Wang, H. Liu, S. Dou, *ACS Nano* **2021**, *15*, 2197. b) L. Jin, C. Shen, Q. Wu, A. Shellikeri, J. Zheng, C. Zhang, J. P. Zheng, *Adv. Sci.* **2021**, *8*, 2005031. c) Z. Huang, Z. Deng, Y. Zhong, M. Xu, S. Li, X. Liu, Y. Zhou, K. Huang, Y. Shen, Y. Huang, *Carbon Energy* **2022**, *4*, 1107.

- [6] a) G. Wang, F. Li, D. Liu, D. Zheng, Y. Luo, D. Qu, T. Ding, D. Qu, *ACS Appl. Mater. Interfaces* **2019**, *11*, 8699. b) R. Ding, S. Tian, K. Zhang, J. Cao, Y. Zheng, W. Tian, X. Wang, L. Wen, L. Wang, G. Liang, *J. Electroanal. Chem.* **2021**, *893*, 115325. c) Y. Shen, X. Shen, M. Yang, J. Qian, Y. Cao, H. Yang, Y. Luo, X. Ai, *Adv. Funct. Mater.* **2021**, *31*, 2101181. d) S. Y. Yang, X. Y. Yue, W. Q. Dai, D. L. Wang, H. Y. Xia, Y. Qiao, Z. W. Fu, *Chem. Commun.* **2021**, *57*, 10371. e) F. Wang, B. Wang, Z. Yu, C. Zhu, P. Liu, J. Li, B. Wang, Y. Zhou, D. Wang, H. K. Liu, S. Dou, *Cell Rep. Phys. Sci.* **2022**, *3*, 100872.
- [7] a) F. Zhou, X. Zhao, P. P. Ferguson, J. S. Thorne, R. A. Dunlap, J. R. Dahn, *J. Electrochem. Soc.* **2008**, *155*, A921. b) X. Liu, L. Yin, D. Ren, L. Wang, Y. Ren, W. Xu, S. Lapidus, H. Wang, X. He, Z. Chen, G.-L. Xu, M. Ouyang, K. Amine, *Nat. Commun.* **2021**, *12*, 4235. c) B. Han, Y. Zhang, C. Liao, S. E. Trask, X. Li, R. Uppuluri, J. T. Vaughey, B. Key, F. Dogan, *ACS Appl. Mater. Interfaces* **2021**, *13*, 28017.
- [8] a) N.-S. Choi, I. A. Profatlova, S.-S. Kim, E.-H. Song, *Thermochim. Acta* **2008**, *480*, 10. b) X. Pu, G. Yang, C. Yu, *Nano Energy* **2014**, *9*, 318. c) O. Vernalis, A. Simone, *Mech. Mater.* **2019**, *136*, 103030.
- [9] a) J. Zhao, Z. Lu, N. Liu, H. W. Lee, M. T. McDowell, Y. Cui, *Nat. Commun.* **2014**, *5*, 5088. b) J. Zhao, Z. Lu, H. Wang, W. Liu, H. W. Lee, K. Yan, D. Zhuo, D. Lin, N. Liu, Y. Cui, *J. Am. Chem. Soc.* **2015**, *137*, 8372. c) X. Li, Y. Li, Y. Tang, L. Zhang, J. Huang, *J. Power Sources* **2021**, *496*, 229868.
- [10] a) J. Li, Z. Kong, X. Liu, B. Zheng, Q. H. Fan, E. Garratt, T. Schuelke, K. Wang, H. Xu, H. Jin, *InfoMat* **2021**, *3*, 1333. b) Q. Man, Y. An, C. Liu, H. Shen, S. Xiong, J. Feng, *J. Energy Chem.* **2023**, *76*, 576.
- [11] a) A. L. Michan, B. S. Parimalam, M. Leskes, R. N. Kerber, T. Yoon, C. P. Grey, B. L. Lucht, *Chem. Mater.* **2016**, *28*, 8149. b) Y. Zheng, Z. Shi, D. Ren, J. Chen, X. Liu, X. Feng, L. Wang, X. Han, L. Lu, X. He, M. Ouyang, *J. Energy Chem.* **2022**, *69*, 593.
- [12] S. Weng, S. Wu, Z. Liu, G. Yang, X. Liu, X. Zhang, C. Zhang, Q. Liu, Y. Huang, Y. Li, M. N. Ateş, D. Su, L. Gu, H. Li, L. Chen, R. Xiao, Z. Wang, X. Wang, *Carbon Energy* **2022**, *5*, 224.
- [13] C. Fang, J. Li, M. Zhang, Y. Zhang, F. Yang, J. Z. Lee, M. H. Lee, J. Alvarado, M. A. Schroeder, Y. Yang, B. Lu, N. Williams, M. Ceja, L. Yang, M. Cai, J. Gu, K. Xu, X. Wang, Y. S. Meng, *Nature* **2019**, *572*, 511.
- [14] a) R. Xu, C. Yan, Y. Xiao, M. Zhao, H. Yuan, J.-Q. Huang, *Energy Storage Mater.* **2020**, *28*, 401. b) W. Fang, Z. Wen, L. Chen, Z. Qin, J. Li, Z. Zheng, Z. Weng, G. Wu, N. Zhang, X. Liu, X. Yuan, G. Chen, *Nano Energy* **2022**, *104*, 107881.
- [15] a) D. Wu, J. He, J. Liu, M. Wu, S. Qi, H. Wang, J. Huang, F. Li, D. Tang, J. Ma, *Adv. Energy Mater.* **2022**, *12*, 2200337. b) N. Qin, L. Jin, Y. Lu, Q. Wu, J. Zheng, C. Zhang, Z. Chen, J. P. Zheng, *Adv. Energy Mater.* **2022**, *12*, 2103402.
- [16] a) Z. Cao, P. Xu, H. Zhai, S. Du, J. Mandal, M. Dontigny, K. Zaghbi, Y. Yang, *Nano Lett.* **2016**, *16*, 7235. b) J. Zhao, L. Liao, F. Shi, T. Lei, G. Chen, A. Pei, J. Sun, K. Yan, G. Zhou, J. Xie, C. Liu, Y. Li, Z. Liang, Z. Bao, Y. Cui, *J. Am. Chem. Soc.* **2017**, *139*, 11550.